RSC Advances

PAPER

View Article Online
View Journal | View Issue

Cite this: *RSC Adv.*, 2024, **14**, 27252

In vitro and *in silico* studies of alpha glucosidase inhibition and antifungal activity of *coffea canephora* husk†

Tran Thi Ngoc Mai,[a] Phan Nhat Minh,[bc] Nguyen Tan Phat,[bc] Mai Thanh Chi,[bc] Dang Chi Hien,[bc] Van-Kieu Nguyen,[de] Thuc Huy Duong,[f] Tran Thanh Nha,[g] Tran Nguyen Minh An,[*h] Nguyen Ngoc Huyen Tran[h] and Mai Dinh Tri*[bc]

The coffea *canephora* husk, a protected agricultural crop, is abundant in Vietnam. Examining the effects of *C. canephora* husk compounds on α-glucosidase and antifungal drug activity was the primary objective of this research. A cholestane-type steroid, coffeacanol A (**1**), was extracted from the ethyl acetate extract. Three cholestane-type derivatives (**2–4**) and three additional known compounds (**5–7**) were separated, and we used a variety of chromatographic techniques to identify a total of six substances. We used NMR to determine the chemical structures of these substances. Extensive HR-MS-ESI analysis and NMR experimental data were used to confirm the structure of the novel metabolite (**1**). The cholestane-type steroid was initially discovered in the *Coffea canephora* husk, marking the first instance in the coffee plant family to reveal chemical structures (**1–7**). The inhibition of α-glucosidase was found to be significantly higher in all compounds tested, with the exception of compounds (**2**) and (**5**). *In vitro*, the positive control showed the lowest inhibition, and the range of IC_{50} values was calculated to be 27.4 to 96.5 μM, which is lower than the IC_{50} value of 214.50 μM for the acarbose control. With an IC_{50} value of 27.4 μM, compound (**7**) showed the greatest capacity to inhibit α-glucosidase among the test compounds. The 3TOP and 2VF5 enzyme crystal structures were used for *in silico* docking investigations and validations of compounds (**1–7**). *In silico* calculations to explain how compound (**7**) shows high activity *in vitro via* the enzyme inhibition mechanism by residual amino acids, like Gly 1102 (B chain) and Glu 1095 (B chain), and their relative interaction with compounds (**7**) and acarbose. Compound (**7**) exhibited the best antifungal activity against *Candida albicans* fungus among three fungi, namely *Candida albicans*, *Trichophyton mentagrophytes*, and *Trichophyton rubrum*, with a MIC value of 25 μM. Compound (**7**) and fluconazole combined to form similar interactions in the contact ligand model, including the functional group, capping group, and linker part, which interacted fully with the 2VF5 enzyme, leading to effective *in vitro* inhibition.

Received 16th June 2024
Accepted 13th August 2024

DOI: 10.1039/d4ra04405c

rsc.li/rsc-advances

1. Introduction

Diabetes, or high blood glucose levels, can lead to neurological, retinal or cardiovascular diseases.[1–3] Inhibition of α-glucosidase or α-amylase could be one of the keys to controlling post-prandial hyperglycaemia.[4–6] Remarkably, the bioactive compounds, phenolic compounds such as chlorogenic acid, trigonelline, anthocyanin, protocatechuic acid, gallic acid, rutin, and caffeine,[7] found in coffee pulps affect several pathways involved in the pathogenesis of type 2 diabetes, reducing the risk of this disease.[8] Especially, the major compounds of the coffee outer skin, caffeic and chlorogenic acid, were recognized as having the α-glucosidase and α-amylase inhibitory potential.[9] Although the coffee showed diverse bioactivities such as antioxidant[10–12] and antibacterial,[10,11] only a few chemical investigations of antidiabetic and antimicrobial activities of

[a]*Institute of Applied Sciences, HUTECH University, 475A Dien Bien Phu Street, Ward 25, Binh Thanh District, Ho Chi Minh City, Vietnam*

[b]*Institute of Chemical Technology, Vietnam Academy of Science and Technology, 1A TL29 Street, Thanh Loc ward, District 12, Ho Chi Minh City, Vietnam. E-mail: maidinhtri@gmail.com*

[c]*Graduate University of Science and Technology, Vietnam Academy of Science and Technology, 18 Hoang Quoc Viet, Cau Giay, Hanoi, Vietnam*

[d]*Institute of Fundamental and Applied Sciences, Duy Tan University, Ho Chi Minh City 700000, Vietnam*

[e]*Faculty of Natural Sciences, Duy Tan University, Da Nang, 550000, Vietnam*

[f]*Department of Chemistry, Ho Chi Minh City University of Education, 280 An Duong Vuong Street, District 5, 748342, Ho Chi Minh City, Vietnam*

[g]*Department of Environmental Engineering, Thu Dau Mot University, Binh Duong, Vietnam*

[h]*Faculty of Chemical Engineering, Industrial University of Ho Chi Minh City, Ho Chi Minh City, 71420, Vietnam. E-mail: tranguyenminhan@iuh.edu.vn*

† Electronic supplementary information (ESI) available: HR-ESIMS, ^{1}H and ^{13}C-NMR, HSQC, HMBC of compound (**1**) and spectroscopic data of compounds (**2**), (**3**), (**4**), (**5**), (**6**), and (**7**) are available in the ESI file. See DOI: https://doi.org/10.1039/d4ra04405c

Coffea canephora husk have been reported.[13,14] Antibacterial activity studies of *Coffea robusta* leaf extract (RLE) showed that chlorogenic acid (CA) is a major component inhibited against *Staphylococcus aureus*, *Bacillus subtilis*, *Escherichia coli*, and *Salmonella typhimurium*.[15] The biological activity mechanism of chlorogenic acid and its applications in the food industry are stated in a review report.[16] Chlorogenic acid involved in on synthesis of the fatty acid in animals and bacteria *via* enzyme catalyst,[17] pharmacological action and potential targets.[18] In the course of the search for new α-glucosidase inhibitors from the *Coffea canephora* husk, waste material in large amounts from Daklak province, Vietnam, we isolated seven compounds, including one new cholestane-type steroid, 24*S*-ethylcholestane-1α,3β-diol, namely coffeacanol A (**1**), along with three steroids, ergosterol peroxide (**2**),[19] cerevisterol (**3**),[20] gramisterol (**4**),[21] one alkaloid, caffeine (**5**),[22] and two phenolics, methyl 5-*O*-caffeoylquinate (**6**),[23] and chlorogenic acid (**7**)[24] from the ethyl acetate extract of the *Coffea canephora* husk. Details of the structural elucidation of (**1**) are presented. Compounds (**1–7**) were further examined for their α-glucosidase inhibition and antifungal activity. Recently, computer-aided drug designing has been applied to predict and discover drug activities *in silico*, and the software Autodock provides the docking of the best conformation of ligands.[25] It is based on scoring functional, generic algorithm (GA), and experimental Gibbs free energy.[26] The validation of the model is performed by the RMSD of ligands to a reference ligand that is available in the enzyme.[27,28] The efficacy of *in silico* docking has been demonstrated in selecting target enzymes more effectively than proteins. Additionally, the publications provide a detailed explanation of the ligand interaction model between the ideal docking position and the target enzyme.[29] Some typical enzymes are chosen to explore the properties, such as antibacterial activity: 2VF5: PDB, anti-inflammatory activity,[30] anticancer based on human topoisomerase I: 1T8I: PDB,[31] antidiabetic activity: 3TOP or 4J5T: PDB[32–36] anti ageing activity ROS (3ZBF: PDB), collagenase (966C: PDB), hyaluronidase (1FCV: PDB) enzyme[37] and others, to calculate docking. The stability of the complex formed by the best docking pose and enzyme has been evaluated using molecular dynamics simulations ranging from 0 to 100 ns in a real environment. These simulations are performed using Gromac or Desmond-Schrodinger software on Ubuntu or Linux.[38–42] The best docking pose of the ligand that showed good activity is usually performed by the ADMET pharmacokinetic model.[33,43–45] In this effort, we isolated, structurally characterised, *in vitro*-glucosidase inhibited, novel antifungal activity, and performed *in silico* molecular docking investigations on the crystal structures of 3TOP (glucosidase inhibition) and 2VF5 (antibacterial activity) from PDB. We also used an *in silico* docking model to explain why the compounds have such high activity *in vitro*, and we confirmed it with RMSD values.[29]

2. Experimental

2.1. Experimental techniques

2.1.1. Plant material. The husk of *Coffea canephora* was collected from Dak Lak province, Vietnam, in January 2022. The scientific name of the plant was authenticated by the botanist Dang Van Son, Institute of Tropical Biology, Vietnam Academy of Science and Technology.

2.1.2. Extraction and isolation. The dried husks of *Coffea canephora* (5.0 kg) were powdered and extracted in ethanol to obtain the crude extract (CCEt). The CCEt extract (400 g) was applied to liquid–liquid extraction with *n*-hexane, chloroform, and EtOAc, respectively, to give the CCH (75 g), CCC (35 g), and CCE (95 g) extracts. The CCE extract was subjected to column chromatography (CC) using normal-phase silica gel, eluting with the *n*-hexane:EtOAc (20 : 1–0 : 1, v/v) solvents and followed by EtOAc : MeOH (20 : 1–5 : 1 v/v) to get eight fractions, denoted as CCE.I–CCE.XIII. CCE.II fraction (12.0 g) was selected for further fractionation by silica gel CC using a solvent system consisting of *n*-hexane: EtOAc (10 : 1–1 : 1, v/v) to afford six fractions CCE.II.1–CCE.II.6. The fraction CCE.II.2 (2.1 g) was chromatographed by silica gel CC using the *n*-hexane-CH_2Cl_2–MeOH (5 : 1 : 0.1, v/v/v) solvent system to afford compounds **2** (15.0 mg) and **4** (11.0 mg). Fraction CCE.II.4 (3.4 g) was further chromatographed using silica gel CC, eluted with *n*-hexane:EtOAc (2 : 1, 1 : 1, 1 : 2, 1 : 5, v/v) mixtures to furnish 4 subfractions (CCE.II.4.1–CCE.II.4). Subfraction CCE.II.4.2 (650 mg) was passed over a silica gel CC using an eluent as *n*-hexane: EtOAc (1 : 1) to afford compounds **1** (5.0 mg) and **3** (9.0 mg). Next, fraction CCE.IV (21 g) was separated by silica gel CC, eluted with a gradient system of CH_2Cl_2–MeOH (30 : 1–0 : 1, v/v) to give five fractions CCE.IV.1–CCE.IV.5. Fraction CCE.IV.2 (5.0 g) was chromatographed on a silica gel column eluting with a gradient of CH_2Cl_2 : MeOH (30 : 1–1 : 1, v/v) yielding six fractions (CCE.IV.2.1–CCE.IV.2.6). The subfraction CCE.IV.5.2.4 (1.5 g) was separated by chromatography on a silica gel column eluting with CH_2Cl_2 : MeOH (20 : 1, v/v) to obtain compound **5** (250 mg). Compounds **6** (9.0 mg) and **7** (25.0 mg) were obtained from fraction CCE.IV.5.5 (1.2 g) by two consecutive silica gel CC: a normal-phase column with a mobile phase as *n*-hexane: CH_2Cl_2 : MeOH (3 : 1 : 0.1 to 1 : 1 : 0.1, v/v/v) and C-18 reverse phase column using a solvent system of MeOH : H_2O (3 : 1, v/v).

Coffeacanol A (**1**): White amorphous powder; $[\alpha]_D^{25}$ −45,8 (*c* 0.05, $CHCl_3$). HRESIMS 433.4020 $[M + H]^+$ was determined to have the formula $C_{29}H_{53}O_2$ (calcd for $C_{29}H_{53}O_2$, 433.4046); ^{1}H-NMR (600 MHz, DMSO-d_6) and ^{13}C-NMR (150 MHz, DMSO-d_6), as seen in Table 1.

2.1.3. α-Glucosidase inhibition assay. The α-glucosidase inhibitory activity was determined according to the modified method of Shai *et al.*, 2011.[46] All of the isolated compounds were measured, and acarbose was used as the positive control. Each sample was evaluated in triplicate.

2.1.4. *In vitro* antibacterial activity. *In vitro* antifungal activity have been performed based on a previous article without any modifications.[47] All compounds (**1–7**) were evaluated for their inhibition activity against fungi *Candida albicans* (*C. albican*), *T. mentagrophytes*, and *T. rubrum* by the disk diffusion method. The fluconazole was used as a standard drug for positive standards, prepared at a concentration of 1 mg mL^{-1}. The microbial test organisms were prepared in an LB broth for 24 hours at 37 °C. Potato Dextrose Agar (PDA) media were used to prepare gel plates for fungi. Each strain was

Table 1 Spectroscopic data of ^{1}H (600 MHz) and ^{13}C (150 MHz) NMR of coffeacanol A (**1**) ($CDCl_3$)[a]

	Compound (**1**)				
	δ_C	δ_H		δ_C	δ_H
1	76.3	3.54 (1H, s)	16	28.4	1.83 (1H, m)
					1.26 (1H, m)
2	34.7	1.60 (2H, m)	17	56.3	1.10 (1H, m)
3	67.8	4.09 (1H, dd, 10.8, 4.8)	18	12.3	0.68 (3H, s)
4	40.9	2.09 (1H, m)	19	17.0	1.18 (3H, s)
		1.60 (1H, m)			
5	30.4	1.73 (1H, m)	20	36.3	1.35 (1H, m)
6	26.4	1.17 (2H, m)	21	18.9	0.91 (3H, d, 6.6)
7	32.6	1.54 (1H, m)	22	34.1	1.32 (1H, m)
		1.41 (1H, m)			1.00 (1H, m)
8	36.3	1.35 (1H, m)	23	31.0	1.86 (1H, m)
					1.53 (1H, m)
9	46.1	1.22 (1H, m)	24	46.0	0.94 (1H, m)
10	38.5	—	25	29.4	1.66 (1H, m)
11	21.3	1.37 (2H, m)	26	19.8	0.81 (3H, d, 6.6)
12	40.1	2.00 (1H, m)	27	19.2	0.83 (3H, d, 6.6)
		1.16 (1H, m)			
13	42.9	—	28	23.3	1.28 (1H, m)
					1.23 (1H, m)
14	56.1	1.08 (1H, m)	29	12.1	0.84 (3H, t, 7.8)
15	24.3	1.57 (1H, m)			
		1.07 (1H, m)			

[a] δ (ppm); J in Hz.

swabbed uniformly into the individual plate using sterile cotton swabs. Paper dishes of 6 mm diameter were placed on PDA disk surfaces. For this step, samples of compounds (**1–7**) at the concentration of 200 to 3.125 μM were taken equally at 30 μL; meanwhile, each fungi sample was added with the positive drug into a paper disk. For every fungus, 30 μL of the sample of compound (**1–7**) and the positive drug were placed on the paper disk. After incubation at 37 °C for 48 hours, the level of the inhibited zone was measured.

The macro-broth dilution assay: the dilution method is employed to continuously conduct *in vitro* experiments with the active compounds. The concentrations of active entries were diluted by a two-fold dilution to obtain a series of highest to lowest concentrations as 200 100, 50, 25, 12.5, 6.25 and 3.125 μM. These sample concentrations of entries (**1–7**) were then incubated in the media culture and fungi solution. The suitable temperature for bacteria was 37 °C for 48 hours. The lowest concentration of the entry, which inhibited the growth of bacteria or fungi, is called the MIC value in units of μM.

2.2. *In silico* techniques

In *silico* docking models were used to explain the high *in vitro* antibacterial activity and alpha glucosidase inhibiton activity of the compounds, which was conducted by Autodock software *via* Scheme 1. To explain the antibacterial activity and alpha glucosidase inhibtion, the enzymes, 2VF5 and 3TOP: PDB, have

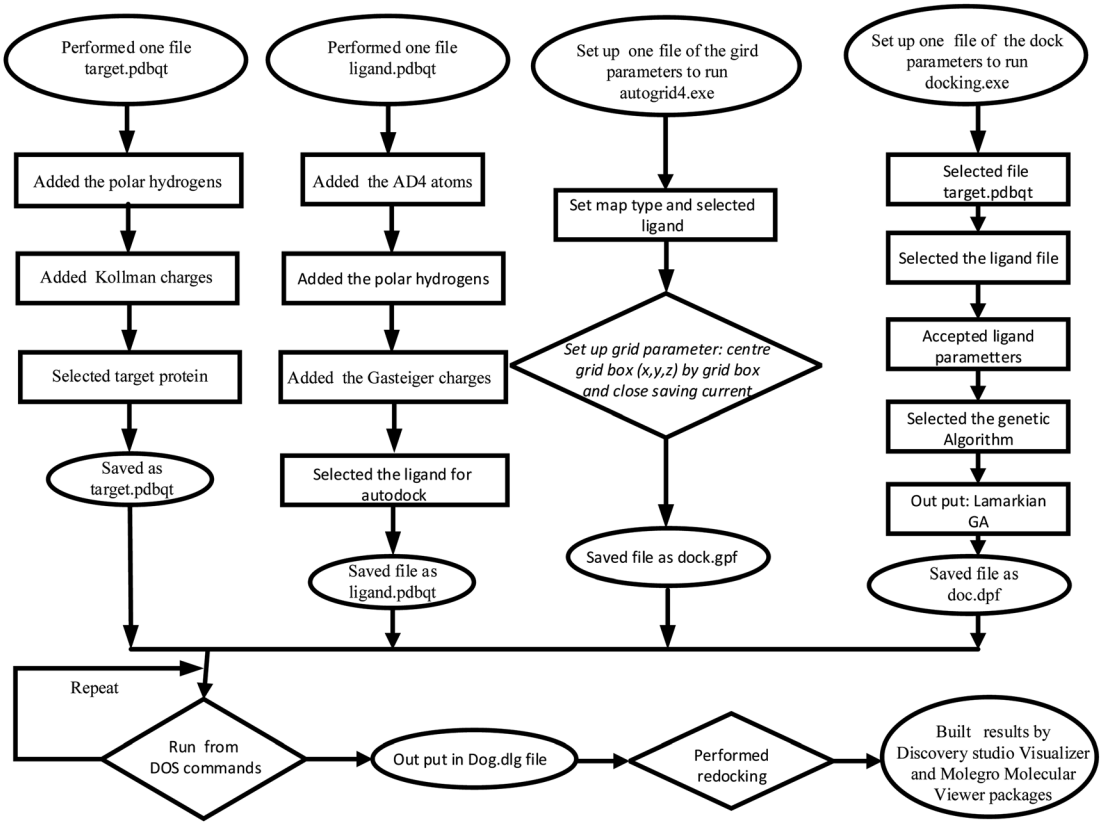

Scheme 1 The docking procedure of the best pose docking of the activity of compounds *in vitro* to an enzyme, such as 3TOP and 2VF5: PDB enzyme.

been used, respectively. For the best pose docking to 2VF5 and 3TOP, the parameters are set in gird files (dock.gpf) such as the numbers in *X*, *Y*, and *Z* axis of (60, 60, 60), spacing of 0.5 Å, and grid center at coordinator of (26.579, 22.731, 8.113); and the numbers of grid points in *X*, *Y*, *Z* axis of (50, 50, and 50), spacing of 0.5 Å, and grid center at coordinator of (−41.385, 12.152, −16.311), respectively. All ligand structures were optimized by Avogadro software version 1.1.1, and structures were saved as filename.pdb before the docking. Structures of ligands were optimized using the MMFF94 force field. For ligands, we applied AD4 methods and ran 500–1000 docking models.[33,48] The coordinates (*X*,*Y*,*Z*) of the active center on the enzyme protein were determined using the Autodock software as per a previous article.[49] Autodock software version 1.5.6rc3 (1099–2011), Discovery Studio Visualizer version v21.1.0.20298 (2021), Molegro molecular viewer version 2.5.0-2012-10-10, Avogadro version 1.1.1, PyMOL software version of non-profit purchase were used for calculations and building the model.

3. Results and discussion

3.1. Chemical characterization

The EtOAc extract from the husks of *C. canephora*, collected at Dak Lak province, was subjected to a normal-phase silica gel column chromatography to provide seven compounds (**1**–**7**), as shown in Fig. 1. Compound (**1**) was obtained as a white amorphous powder. The formula for HR-ESI-MS data *m*/*z* 433.4020 $[M + H]^+$ was determined as $C_{29}H_{52}O_2$. The ^{1}H-NMR spectrum of (**1**) showed two oxygenated methine protons at δ_H 3.54 (1H, brs, H-1), 4.09 (1H, dd, J = 10.8, 4.8 Hz, H-3), and six methyl groups at δ_H 0.68 (3H, s, H-18), 1.18 (3H, s, H-19), 0.91 (3H, d, J = 6.6 Hz, H-21), 0.81 (3H, d, J = 6.6 Hz, H-26), 0.83 (3H, d, J = 6.6 Hz, H-27), and 0.84 (3H, t, J = 7.8 Hz, H-29) as indicated in Table 1. The ^{13}C-NMR and HSQC spectroscopy of compound (**1**) exhibited twenty-nine carbons, including two oxygenated methine carbons at δ_C 76.3 (C-1), 67.8 (C-3), two quaternary carbons, eleven methylene carbons, eight methine carbons, and six methyl carbons at δ_C 12.3 (C-18), 17.0 (C-19), δ_C 18.9 (C-21), 19.8 (C-26), 19.2 (C-27), and 12.1 (C-29). These results confirm that compound (**1**) is a cholestane-type skeleton, bearing two hydroxyl moieties located at C-1 and C-3, further supported by the HMBC correlation of H-10 to C-1 (δ_C 76.3) along with both H-1 (δ_H 3.54) and H_2-2 (δ_H 1.60) to C-3 (δ_C 67.8).

Additionally, the occurrence of a triplet methyl signal at δ_H 0.84 (3H, t, J = 7.8 Hz) led to the presence of an ethyl moiety, which could be located at C-24 based on the HMBC correlation of H_3-29 (δ_H 0.84) to both methine carbon C-24 (δ_C 46.0) and methylene carbon C-28 (δ_C 23.3), as seen in Fig. S2.† As to the relative configuration, the multiplicities and J coupling constants of two oxygenated methine protons H-1 and H-3 at δ_H 3.54 (1H, brs, H-1), and 4.09 (1H, dd, J = 10.8, 4.8 Hz, H-3) indicate 1α and 3β orientations of two OH groups at carbons

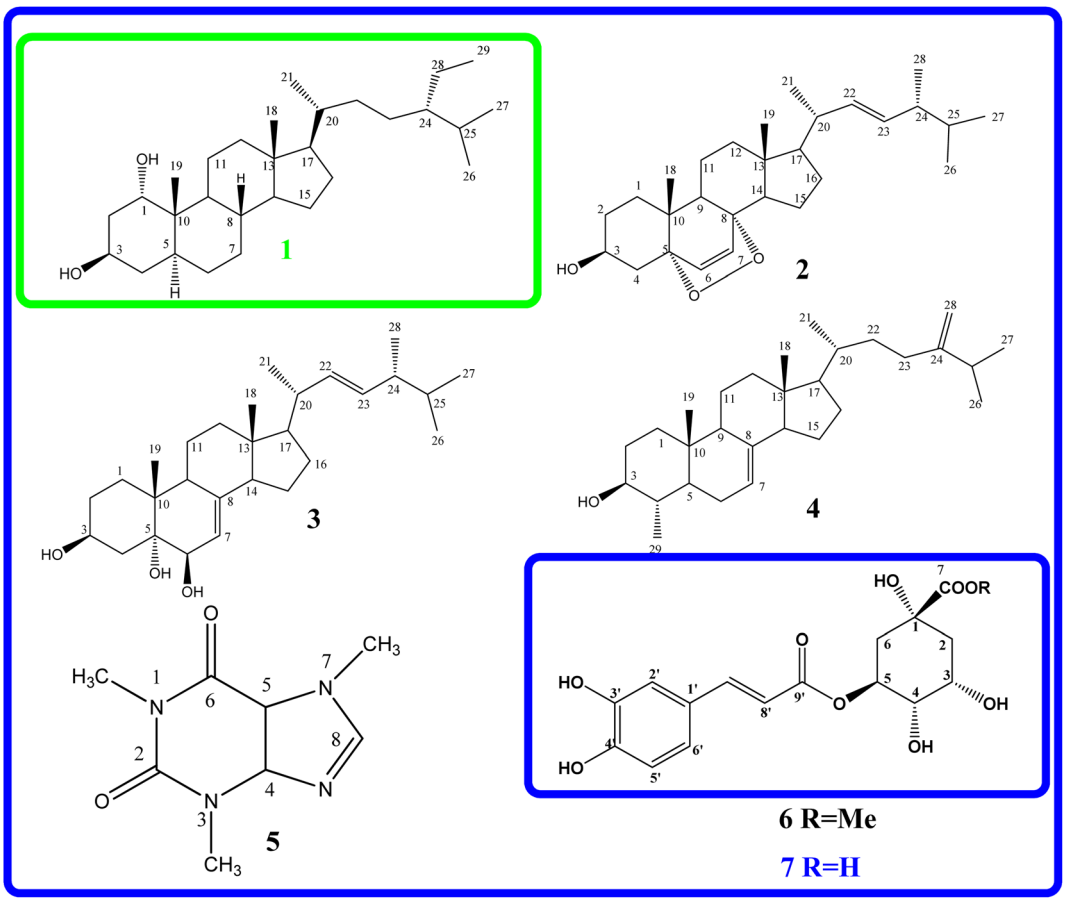

Fig. 1 Molecular structure of compounds isolated from the husk of *Coffea canephora*.

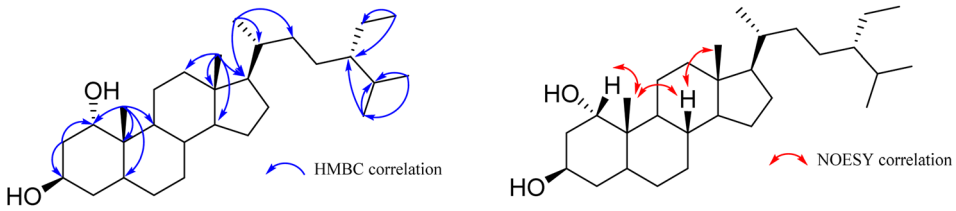

Fig. 2 The HMBC and NOESY correlations of compound (1).

Table 2 The values of RMSD of pair poses between the best pose 235 *in silico* and *in vitro* and another compound such as poses 119, 155, 237, 355, 394, and 493

RMSD of pose (a, b)[c], Å	119[b], green	155, cyan	237, yellow	355, gray	394, deep blue	493, red
235[a], violet	2.25	2.50	1.93	2.42	3.18	2.59

[a] Reference pose. [b] The best docking pose of the compound. [c] RMSDs value are calculated based on the PyMOL software.

C-1 and C-3, respectively. Furthermore, the ^{13}C NMR data comparison of compound (**1**) with those of 24*S*-methylcholesterol, 24*S*-methylcholestan-1,3-diol, 24*S*-methylcholestan-11-acetoxy-1,3,5,6-tetraol, and 3,5,25-trihydroxy-24*S*-methylcholestan-6-one[50] led to the illustration of the 24*S* configuration of compound (**1**). Moreover, the NOESY correlations of H-1/H_3-19, H_3-19/H-8, and H-8/H_3-18 supported the β faces of these protons, as seen in Fig. 2. Thus, the chemical structure of compound (**1**), namely coffeacanol A, was established as 24*S*-ethylcholestane-1α,3β-diol. All isolated compounds (**1–7**) were investigated for the *in vitro* studies of enzyme inhibitory against α-glucosidase, as seen in Table 2. Acarbose was used as a positive control with an IC_{50} value of 214.5 μM. As per the results, compounds (**1**), (**3**), (**4**), (**6**), and (**7**) display good inhibitory effects, with IC_{50} values in the range from 27.4 to 96.5 μM. It is worth noting that all of these isolated compounds were first reported from the *Coffea canephora* husk.

3.2. *In vitro* α-glucosidase activity

All compounds (**1–7**) and positive control (Acarbose) were analyzed for alpha glucosidase inhibition *in vitro*, as seen in Fig. 3; compound (**7**) indicated the most alpha glucosidase inhibitor activity with the value of IC_{50} of 27.4 μM among the test entries. This value is 8-fold less than that of compounds (**1–7**) and the positive control (Acarbose), as evaluated for the α-glucosidase inhibition *in vitro* illustrated in Fig. 3. Compound (**7**) had the highest level of α-glucosidase inhibitor activity, with an IC_{50} value of 27.4 μM, among all the compounds tested. The value of this molecule is 8 times lower than that of acarbose, and compound (**7**) inhibited α-glucosidase more effectively than acarbose by a ratio of 8. The compounds' inhibitory properties have been classified in the following order: compound (**5**), compound (**2**), Acarbose (**4**), compound (**1**), compound (**3**), compound (**6**), and compound (**7**). The inhibition effects of entry compounds against α-glucosidase have been demonstrated *in silico* docking model based on the optimal docking position of compound (**7**), which exhibited good docking performance in experimental *silico*. The inhibition observed against α-glucosidase has been revealed by the utilization of an *in silico* docking model. Previous reports have indicated that coffee plants, specifically C. arabica, exhibit α-glucosidase inhibition.[13] Caffeine (**5**) was believed to be a bioactive inhibitor against alpha glucosidase, *i.e.*, *C. arabica*.[51] *In silico* and *in vitro* inhibition of ergosterol peroxide (**2**) was reported, the data of which are consistent with our investigation.[52] Chlorogenic acid (**7**) was believed to be a potent candidate for treating type-2 diabetes.[14,53] As far as we know, this is the first report of the inhibition of α-glucosidase (both *in vitro* and *in silico*) by compounds (**3-4**) and (**6**).

3.3. *In silico* docking model of alpha glucosidase inhibition activity

3.3.1. Docking model of active poses/active ligands to the crystal structure of 3TOP: PDB enzyme. Table 4S, Fig. 4, 5 and S31–S37† show the *in silico* computational results for

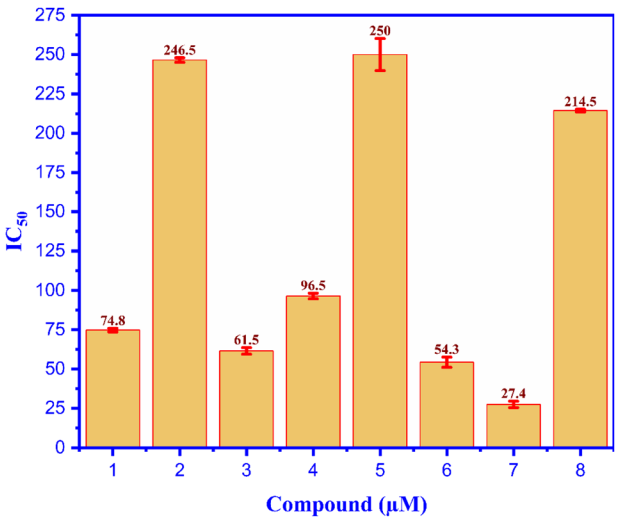

Fig. 3 The alpha glucosidase activity of compounds **1–7** and (**8**): acarbose *in vitro* test.

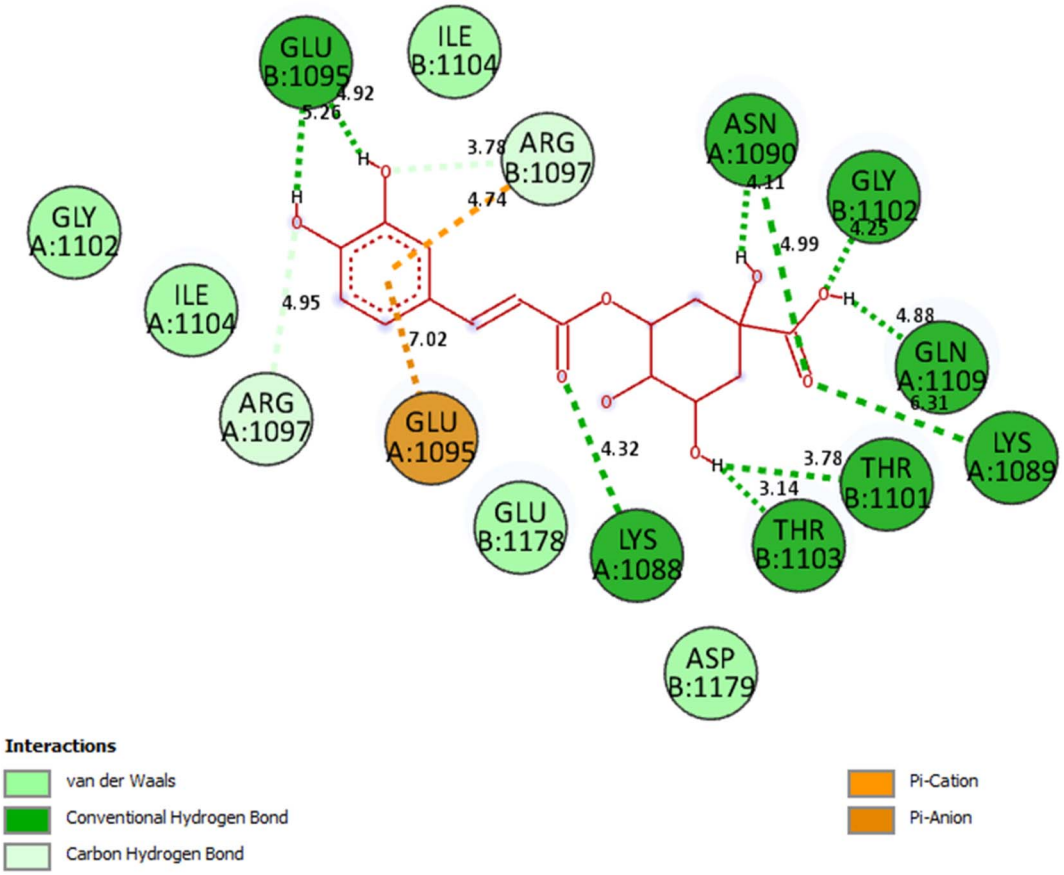

Fig. 4 The significant ligand interactions between compound **7** and residual amino acid on the crystal structure of 3TOP: PDB enzyme, hydrogen bondings: dark green color, yellow color: pi cation interactions.

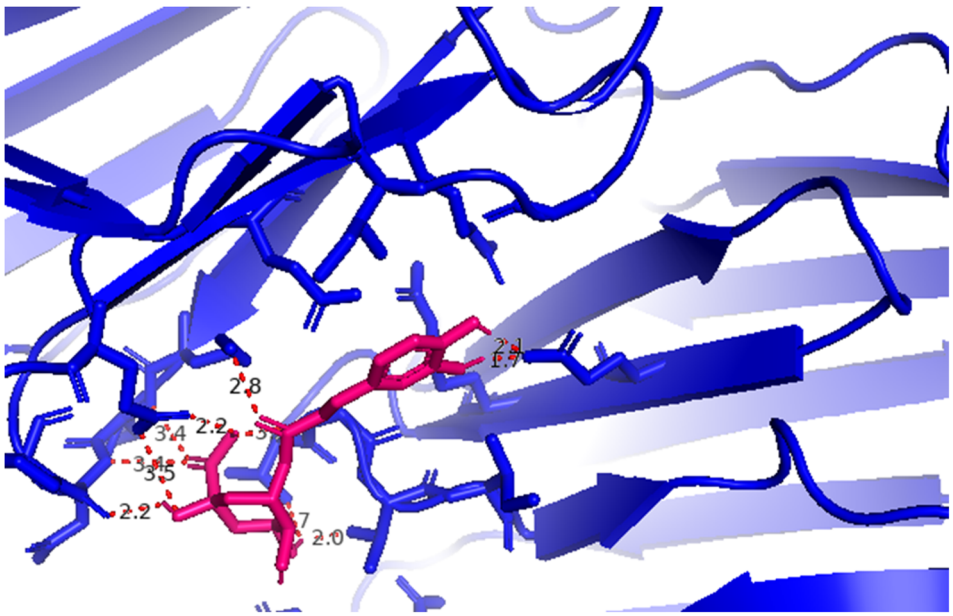

Fig. 5 A 3D image from PyMOL software presenting the hydrogen bonding forming around compound **7**; red color (compound **5**), green color: crystal structure of 3TOP enzyme.

compounds (**1**–**7**). The optimal docking postures of molecules with the thermodynamic data (free Gibb energy, ΔG°, at 25 K and $P = 1$ atm) are organized in the following sequence, as shown in Table 4S:† compound (**1**)/pose 491 > compound (**6**)/pose 394 > compound (**7**)/pose 235 > compound (**5**)/pose 355 > compound (**4**)/pose 237 > compound (**3**)/pose 119 > compound (**2**)/pose 155. The best docking poses are docked to the same enzyme, 3TOP: PDB, based on the values of the inhibition constants or Gibbs free energy. One pose interacts well with the 3TOP enzyme mostly because of the ligand interaction model, which is the secondary component. When there are three components to a docking posture—a functional group or binding group (FG), a capping group, and a connecting unit (CU) or linker—that interact well with the enzyme, the docking pose has an excellent relationship with the enzyme in the interaction model.[29]

Compound (7) or pose 235: As seen in Fig. 4, 5 and Table 4S,† pose 235 attaches to the crystal structure of the 3TOP enzyme with Gibbs free energy and inhibitory constant values of −4.98 kcal mol^{-1} and 224.1 M, respectively. Together with the remaining amino acids on 3TOP, Lys 1088, Gln 1109, Glu 1095, Thr 1103, and Asn 1090 created eight hydrogen bonds. Because of its short bond length, hydrogen bonding pose 235: H–B: Glu 1095: O (1.71 Å) is the most stable among them. Because three components of pose 235 demonstrated comprehensive interactions with 3TOP, as shown in Table 4S† and Fig. 4, pose 235 interacted with 3TOP. Fig. 5 demonstrates the formation of 11 hydrogen bonds (red color line) between compound 7 (magenta color) and 3TOP enzyme (blue color). The bonding lengths of the compounds are 2.0, 2.1, 2.2 (**2**), 2.7, 2.8, 3.3, 3.4 (**2**), and 3.5 from the PyMOL software, and these contacts were strong and hydrophilic. Because the three components of compound 7 fully interacted with 3TOP, it had a good interaction with 3TOP. Pose 235's functional groups create hydrogen bonds with Glu 1095: The following are linked: Gln 1109: A to the hydrogen atom of the hydroxyl phenolic ring; Gly 1102: B to the hydrogen atom of the hydroxyl phenolic ring; Lys 1088: A chain to the oxygen atom of the carbonyl group; Thr 1103 and Thr 1101: B to the hydrogen atom of the hydroxyl alcohol; Lys 1089: A to the oxygen atom of the double C=O of carboxylic acid; and Asn 1090: A to the hydrogen atom of the hydroxyl alcohol. The capping group (CA) is connected to the pi-electron system of the phenyl group by Glu 1095: A and pi cation or pi anion interactions. A pi cation or pi anion contact is formed by the linking unit, or linker portion, between Arg 1097: B and the phenyl group's pi-electron system.

Compound (**3**) or pose 119: as shown in Table 4S and Fig. 31S,† pose 119 interacted strongly with the 3TOP enzyme, with Gibbs free energy and inhibition constants of −8.84 kcal mol^{-1} and 0.330 μM. Table 4S† shows that four hydrogen bonds were established with 3TOP. Based on Table 4S,† it can be inferred that this pose has a good interaction with 3TOP because three sections of the pose fully interact with 3TOP. Compound **3** docked well to 3TOP, as shown in Fig. 31S,† because three parts of this pose interacted fully with 3 TOP: Asn 1090, Thr 1103 to hydrogen atoms of the alcohol group in FG; Lys 1088 to the cyclohexane ring in CA; and Ile 1104 to the cyclopentane ring in CU on pose 119. Fig. 37S† illustrates how successfully the positive control medication, acarbose, interacted with 3TOP.

Compound (**6**) or pose 394: as demonstrated in Table 4S and Fig. 32S,† compound 6/pose 394 has been docked to 3TOP with the values of Gibbs free energy and inhibition constant of −5.38 kcal mol^{-1} and 114.0 μM, respectively. It also formed 11 hydrogen bonds with the enzyme, as seen in Table 4S.† In the ligand interaction model, the functional group of pose 394 formed hydrogen bondings from Asp 1107, Lys 1088, Glu 1095; Gln 1109, and Ile 1104 to hydrogen atoms of hydroxyl alcohol, hydroxyl phenolic ring, and oxygen atom of conjugation carbonyl. The connecting unit has one carbon–hydrogen bond from Arg 1097: B to the oxygen atom of the alcohol group on pose 394. The capping group has no hydrophobic interaction.

Compound (**1**) or pose 491: as demonstrated in Table 4S and Fig. 33S,† pose 491 has been anchored to the 3TOP enzyme with the values of free Gibbs energy and inhibition constant of −8.43 kcal mol^{-1} and 0.657 μM, respectively. It has no hydrogen bonding with residual amino acid on the enzyme. In the ligand interaction model, the functional groups have hydrogen bondings from Glu 1095: A and Glu 1095: B to the hydrogen atom of hydroxyl alcohol. The connecting unit shows hydrophobic interaction from Ile 1104 to the cycloalkane ring but the capping group has no interaction. We conclude that pose 491 has not interacted well with the enzyme because 3 parts of pose 491 did not interact fully with the enzyme.

Compound (**4**) or pose 237: as indicated in Table 4S and Fig. 34S,† pose 237 linked to the 3TOP enzyme with the values of Gibbs free energy and inhibition constant of −9.49 kcal mol^{-1} and 0.11 μM, respectively. This pose also formed one hydrogen bond with residual amino acids on the enzyme. In the ligand interaction model, as indicated in Fig. 34S,† the functional group of this pose showed one hydrogen bond from Asn 1090 to the hydrogen atom of hydroxyl of the alcohol group. The connecting unit (CU) of the pose has one alkyl interaction from Ile 1104 to the cyclopentane ring. The capping group has no interaction. Pose 237 did not interact well with the enzyme because of no interactions with the capping group (CA).

Compound (**2**) or pose 155: as indicated in Table 4S and Fig. 35S,† pose 155 docked to the 3TOP enzyme with the values of Gibbs free energy and inhibition constant of −8.71 kcal mol^{-1} and 0.412 μM, respectively. This pose showed one hydrogen bonding from Gln: 1109: B chain to the hydrogen atom on the pose. As demonstrated in Fig. 35S,† the functional group of pose 155 has one hydrogen bonding and hydrophilic interaction from Gln 1109 to the hydrogen atom of the hydroxyl group of alcohol. The capping group of the pose showed one carbon–hydrogen bond from Glu 1095: A to the oxygen atom of the peroxide ring. The connecting unit (CU) has no interaction. Pose 115 has not interacted fully to 3TOP enzyme.

Compound **5** or pose 355: as indicated in Table 4S and Fig. 36S,† pose 355 anchored to the 3TOP enzyme with the values of Gibbs free energy and inhibition constant of −4.59 kcal mol^{-1} and 429.8 μM, respectively. As indicated in Fig. 36S,† significant interactions between pose 355 and 3TOP are shown as the functional group of the pose has no hydrogen bonding. The capping group has four carbon–hydrogen bonds,

hydrophobic interactions from Ser 1100, Ile 1087, Lys 1099, and Tyr 1010 to the carbon of methyl group; one carbon–hydrogen bonding from Gln 1081 to the carbon of methyl group; one pi–sigma interaction from Tyr 1010 to the carbon atom of methyl group. The capping group of pose 355 is without detection. Pose 355 did not interact fully with the 3TOP enzyme.

Acarbose or pose 61: as seen in Table 4S and Fig. 37S,† pose 61 has been anchored to 3TOP with values of Gibbs free energy and inhibition constant of −8.81 kcal mol^{-1}, respectively. The significant interactions between pose 61 and 3TOP are presented on a 2D diagram, as shown in Fig. 37S.† The functional group of pose 61 has three hydrogen bonds from Gly 1102: B chain, Gln 1109: B, and Glu 1095. The capping group of the pose are Gly 1102: A and Glu 1095: B to carbons of the carbohydrate, Arg 1097: A chain to the oxygen atom of methylene group on carbohydrate. Connecting units (CU) are Thr 1101: A and Arg 1097: B to the methylene carbon atom and the oxygen atom of the methylene group on the carbohydrate group. Pose 61 is considered as a good interaction in the ligand interaction model.

As seen in Fig. 32S to 36S and Table S4,† compounds (**6**)/pose 394, compound (**1**)/pose 491, compound (**4**)/pose 237, compound (**2**)/pose 155, and compound (**5**)/pose 355 did not fully interact with 3TOP in the ligand interaction model. From the thermodynamic data ($\Delta G°$, K_i), compound (7)/pose 235 docked better than compound (**3**)/pose 119. Compound (7)/pose 235 connected with 3TOP more effectively than compound (**3**)/pose 119 in the ligand interaction model. The 8 and 4 hydrogen bondings, respectively, that link pose 235 and 119 to the 3TOP enzyme support this. Hydrogen bondings are the most significant conformational features in terms of solubility, absorption, distribution, and metabolism in ADMET and MD simulations. The results of α-glucosidase inhibition *in vitro* are comparable to the *in silico* docking model. Fig. 4 and 37S† show the results of the similarity study in the ligand interaction model between pose compound (7)/235 and acarbose/pose 61 with TOP enzyme. These residual amino acids include Gly 1102 (B chain) and Glu 1095 (B chain).

3.3.2. The validation of the docking model to the 3TOP enzyme. The measurement of the RMSD between the compound's optimal docking position and the reference pose, pose 235, is used to validate the docking model. This is because, as Table 2 and Fig. 6 demonstrate, this pose demonstrates the highest α-glucosidase inhibitory activity both *in vitro* and *in silico*. As can be seen in Table 2, the values of pair poses are shown as RMSDs in units of Å. These values fall within the range that is allowed to be used to predict the active center, docking orientation, docking parameters, and docking outcomes. The fact that pose 235's RMSD value is outside of the range indicates that the posture 235 conformation is susceptible to numerous docking procedure modifications. Because acarbose and compound 7 have different structures with respect to the amount of heavy atoms, there is an inaccuracy in the alignment of pose 235 (compound 7) to pose 61 (acarbose).

3.4. *In vitro* antibacterial activity

All compounds (**1**–7) were screened for antifungal activity against *C. alibican*, *T. rubrum*, and *M. gypseum in vitro*, as shown in Fig. 7A and B. Compound (7) shows the most excellent antifungal activity against *C. allicin* at a MIC value of 25 μM among the tested samples. This MIC value of compound (7) is determined to be higher than that of fluconazole. Compound (**6**) indicated high activity against *C. Albian* at a MIC value of 37.5 μM, compared to the MIC of compound (7), which is higher. For *C. allicin*, the ability of antifungal activity is determined as fluconazole (**8**) > compound (7) > compound (**6**) > compound (**5**) = compound (**1**) > compound (**2**) > compound (**3**) > compound (**4**), as seen in Fig. 7B (orange columns). For *T. rubrum* fungi, compound (**4**) indicated moderate activity with a MIC value of 175 μM among the test entries and the highest activity among compounds. The antifungal activity of compound (7) is similar to that of compound (**6**), with a MIC value of 100 μM against *M. gypseum*, and compound (**6**) and (7) also exhibited high fungal activity among test entries against *T. rubrum* fungi. For *M. gypseum* fungi, most of the compounds have shown moderate activity; among them, compounds (7) and (**6**) inhibited highly at MIC values of 100 μM. The antibacterial and antibiofilm activities of chlorogenic acid (CA)/compound (7) against *Yersinia enterocolitica* (*Y. enterocolitica*) were tested, and its mechanism of action was explained in the previous article.[54] Chlorogenic acid showed inhibition against the Gram-negative bacterium *Escherichia coli* IFO 3301.[55] Our work shows its excellent antifungal activity against *C. albican* at the MIC of 25 μM for the first time and also explains the mechanism of excellent inhibition of compound (7) against *C. albican* fungi from the *in silico* docking part as given below.[29]

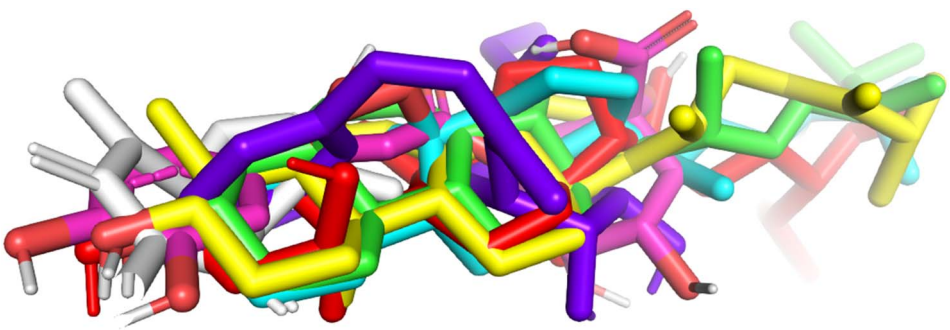

Fig. 6 The poses of compounds aligned to the pose-235, compound 7.

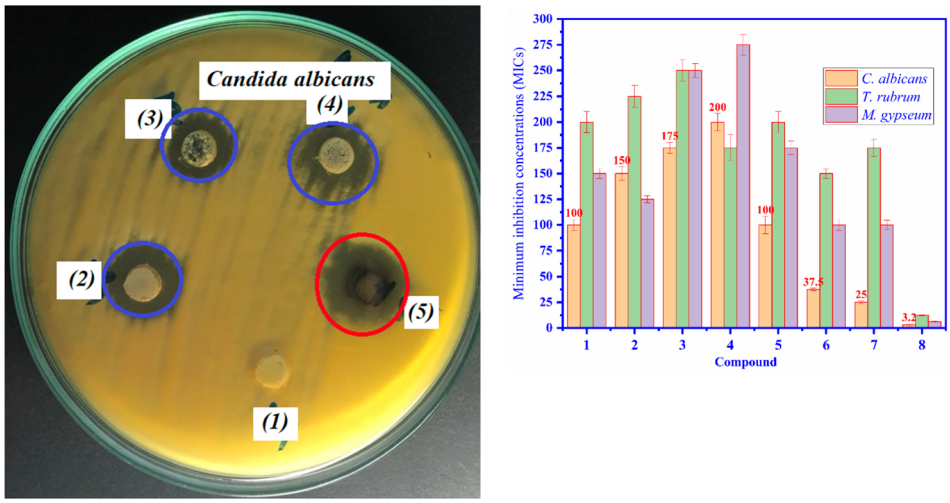

Fig. 7 One petri dish indicated the antifungal activity of compound (7) against *C. albicans* at different concentrations of (1): DMSO solvent, (2): 1000 μM, (3): 500 μM, (4) 250 μM, and (5): fluconazole, 100 μM and graph presented compounds (1–7), and (8): fluconazole-positive control against *C. albican*, *T. rubrum*, and *M. gyseum in vitro*.

3.5. *In silico* docking model of the antibacterial activity

3.5.1. Docking model of active poses/active ligands to the crystal structure of 2VF5 enzyme. All the best docking poses of compounds (1–7) are selected and docked to the crystal structure of the 2VF5 enzyme to explain why compounds show high activity against fungi *via* the mechanism of 2VF5 enzyme inhibition. The significant interactions are calculated and presented in Table 5S, Fig. 8, 9, 38S and 39S.†

Compound 7/pose 49: the best conformation of compound (7) among 1000 docking conformations has been docked to 2VF5 with the values of Gibbs free energy and inhibition constant of −5.25 kcal mol^{-1} and 140 μM, respectively, as seen in Table 5S.† This pose formed eight hydrogen bonds with

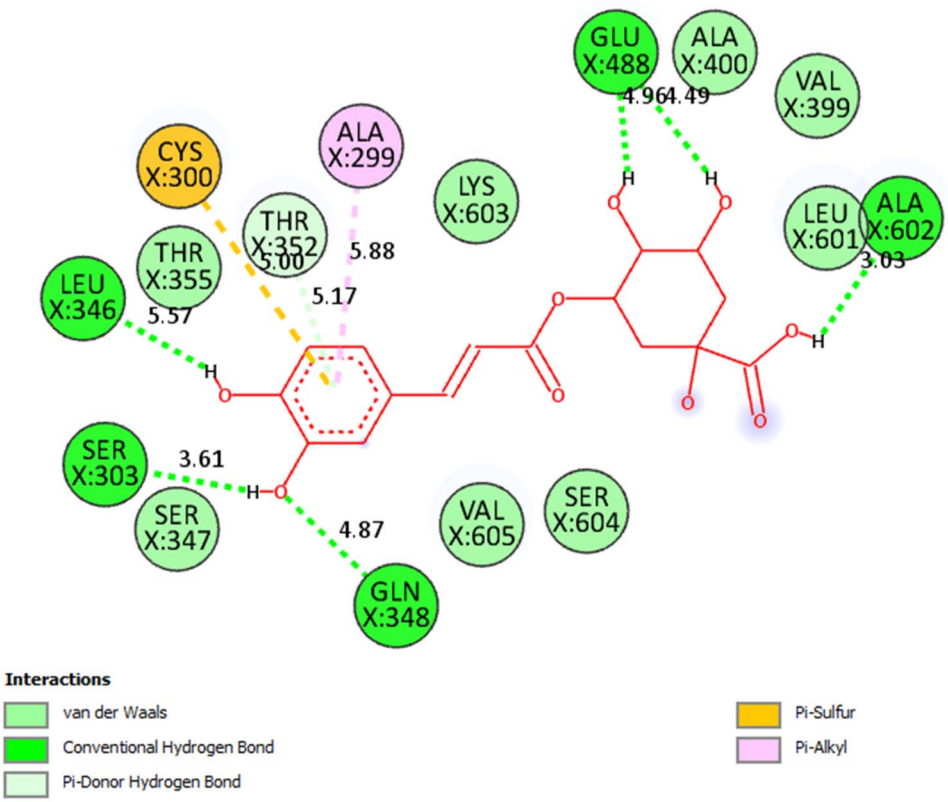

Fig. 8 The significant interactions between the pose 49/compound (7) and residual amino acids on 2VF5 enzyme: PDB based on 2D interaction model: full ligand interactions.

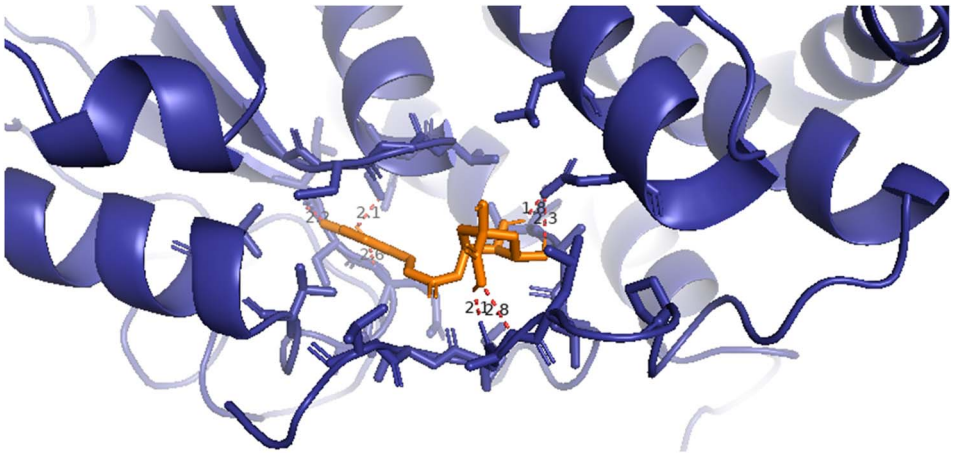

Fig. 9 A 3D image presenting the hydrogen bondings forming around compound 7 by PyMOL software, orange color: compound 7/pose 49, dark blue color: crystal structure of 2VF5 enzyme, red color lines: hydrogen bondings, and the numbers: bond lengths of hydrogen.

residual amino acids, as seen in Table 5S.† Among them, the hydrogen bonding, pose 49:H-XX: Glu 488: O (1.79 Å), has the strongest strength due to its shortest bonding length. This pose showed good interaction because three parts of pose 49 interacted well with enzymes. As seen in Fig. 8, all significant interactions between pose 49 and 2VF5 are indicated in a 2D diagram, including functional groups: 6 hydrogen bondings from Leu 346 to the hydrogen atom of the hydroxyl phenolic group, Gln 348 and Ser 303 to the oxygen atom and hydrogen atom of the hydroxyl phenolic group, respectively, Ala 602 to the hydrogen atom of the hydroxy of carboxylic acid, and Glu 488 to two hydrogen atoms of two hydroxyl alcohols. The capping group has one pi–sulfur interaction from Cys 300 to the system of pi electrons of the phenyl ring and one pi–alkyl interaction from Ala 299 to the system of pi electrons of the phenyl ring. The linker part has one pi–donor hydrogen bond from Thr 352 to a system of pi electrons in the phenyl ring. Compound 7 interacted well with 2VF5 in the ligand interaction model. As shown in Fig. 9, the 3D image by PyMOL software demonstrated the hydrogen bonds forming around compound 7/pose 49. The bonding lengths are 1.8, 2.1 (×2), 2.2, 2.6, 2.3, and 2.8 Å. These hydrogen bondings made around compound (7) proved the interactions between compound (7) and 2VF5: enzymes are very strong and hydrophilic interactions, indicating that compound (7) inhibited the 2VF5 enzyme strongly *in vitro*.

Compound **6**/pose 992: it is anchored to 2VF5 with the values of Gibbs free energy and inhibition constant of −6.81 kcal mol^{-1} and 10.26 μM, as indicated in Table 5S.† Compound (**6**) formed 12 hydrogen bonds with the 2VF5 enzyme, proving the hydrophilic character of compound (**6**). As seen in Fig. 38S,† the significant interactions between pose 992 and 2VF5 are indicated, including functional groups that are hydrogen bondings from Ser 349 and Ser 347 to the oxygen atom of the hydroxyl alcohol group, Thr 352 to the hydrogen atoms of the hydroxyl alcohol groups, Lys 603 to the oxygen atom of the double bonding of C=O, and Ser 303 to the oxygen atom of the methoxy ester group. The capping groups (CA) are pi anion interactions from Gly 488 and pi–alkyl interactions from Leu 601 to the system of pi electrons of the phenyl group. The linker part formed the carbon–hydrogen bonds from Gly 408 to the methyl ester group and Thr 302 to the oxygen atom of the ester group. Compound (**6**) has been considered to have good interactions or inhibitions against enzymes.

Fluconazole (drug)/pose 81: it has docked to 2VF5 with the values of Gibbs free energy and inhibition constant of −5.74 kcal mol^{-1} and 61.85 μM, as indicated in Table 5S† and formed six hydrogen bondings to residual amino acids on the enzyme. As shown in Fig. 39S,† fluconazole interacted well with the enzyme because three parts of the molecule are identified by functional groups: hydrogen bondings from Ser 303 to the oxygen atom of the hydroxyl alcohol group and nitrogen bondings from Cys 300 to another nitrogen atom of the 1,2,4-triazole group. Especially in this pose, there are three halogen bondings from Glu 488, Val 399, and Lys 603 to the fluorine atoms of the phenyl group. The capping groups are discovered *via* one pi–sulfur bonding from Cys 300 to the system of pi electrons of the 1,2,4-triazole group, one pi–alkyl bonding from Ala 299 to the system of pi electrons of the 1,2,4-triazole group, and one pi–alkyl bonding from Ala 404 to the system of pi electrons of another 1,2,4-triazole group. The connecting units are detected *via* one pi–donor hydrogen bonding from Leu 346 and Thr 352 to carbon atoms (sp^2) and a system of pi electrons of the 1,2,4-triazole group, and the pi–donor hydrogen bindings from Ser 401, Gln 408, and Ser 303 to the system of pi electrons of another 1,2,4-triazole group. Other poses, such as pose 720 (compound **1**), compound **2** (pose 329), pose 830 (compound **3**), pose 973 (compound **4**), and pose 177 (compound **5**), have not interacted well with 2VF5 because of a lack of interactions. Compound (7) and fluconazole have similar interactions in three parts, such as the functional groups: hydrogen bondings: Ser 303; capping group: one pi–sulfur interaction: Cys 300 and one pi-alkyl: Ala 219; and connecting unit: pi–donor hydrogen: Thr 352. It has been proved that compound 7 inhibited 2VF5, similar to a fluconazole drug by *in silico* docking.

3.5.2. The validation of the docking model to the 2VF5 enzyme. The best docking pose of every compound has been

Table 3 The values of RMSD of pair poses between the best docking pose of compounds and reference pose, pose 81, and fluconazole by PyMOL software

RMSD of pose (a, b)[c], Å	49[b], blue	992, pink	720, yellow	329, cyan	930, green	973, orange	177, gray
81[a], red color	2.032	2.575	2.623	2.526	2.541	2.591	2.515

[a] Reference pose. [b] The best docking pose of the compound. [c] Values of RMSD are calculated based on PyMOL software.

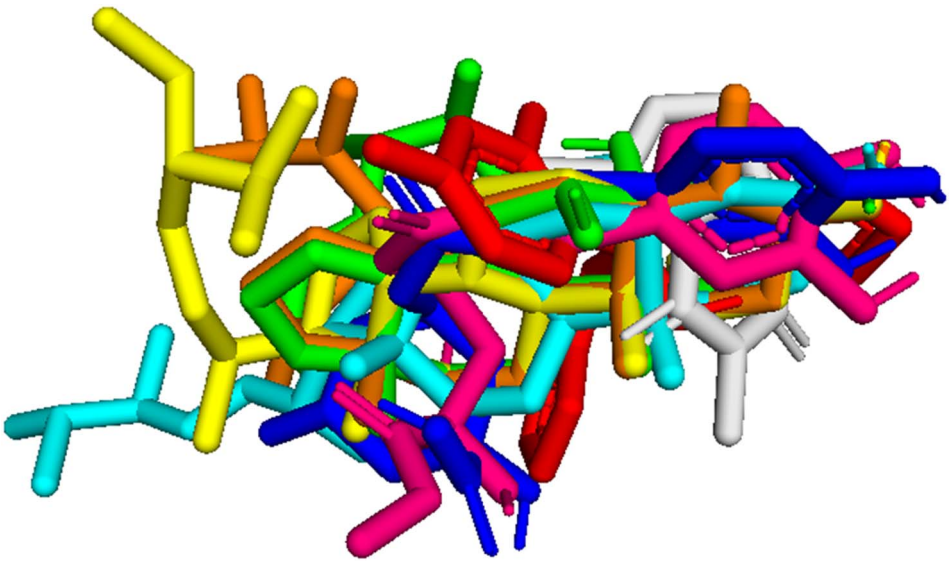

Fig. 10 The docking poses of compounds have aligned to the reference pose, pose 81, and the best docking pose of the control drug, fluconazole.

aligned to the reference pose, pose 81, the best docking pose of fluconazole, the control drug for antifungal activity. The RMSD of the pair poses serves to validate the docking model in terms of docking orientation, docking conformation, the active center or pocket enzyme on 2VF5, and the thermodynamic site values. PyMOL software calculates and builds the values of RMSD for pair poses, as shown in Table 3 and Fig. 10. Among them, the RMSD values of pair poses (pose 49, compound (7), reference pose 81/fluconazole) are 2.032, and this value is the lowest among other pair poses, which proves that pose 49/compound (7) aligned well with pose 81/fluconazole.

4. Conclusion

A novel cholestane-type steroid, Coffeacanol A (**1**), has been identified in the ethyl acetate extract of *Coffea canephora* husk. In addition, six identified chemicals were isolated: ergosterol peroxide (**2**), reregistered (**3**), gramisterol (**4**), caffeine (**5**), methyl 5-*O*-caffeoylquinate (**6**), and chlorogenic acid (7). According to our present knowledge, the outer covering of *Coffea canephors* is the first source of documentation for all the detected chemicals. Compounds (**1**), (**3**), (**4**), (**6**), and (7) demonstrated significant action against α-glucosidase, with IC_{50} values of 74.8, 61.5, 96.5, 54.3, and 27.4 μM, respectively. By comparison, the IC_{50} value of acarbose was 214.5 μM. Compound (7) exhibited remarkable inhibitor efficacy against the alpha glucosidase, both *in vitro* and *in silico*. The amino acids Gly 1102 (B chain) and Glu 1095 (B chain) of the 3TOP: PDB were involved in the ligand interactions between compound (7) or acarbose and 3TOP. This research unequivocally supports the notion that coffee husk reduces the likelihood of developing type 2 diabetes as a result of its bioactive components. Compound (7) showed strongest inhibition activity against *Candida albicans in vitro*, with MIC value of 25 μM. In the *in silico* ligand interaction model, compound (7)/pose 49 and fluconazole drug/pose 81 demonstrated equivalent ligand interactions such as the functional groups of poses-one hydrogen bonding involving serine 303, the capping group: one pi–sulfur contact with cysteine 300 and one pi–alkyl interaction with alanine 219 and the connecting unit: one pi–donor hydrogen with threonine 352.

Data availability

The data supporting this article have been included as part of the ESI.†

Author contributions

Tran Thi Ngoc Mai: conceptualization, methodology. Tran Nguyen Minh An, Mai Dinh Tri: writing – original draft preparation, writing – reviewing and editing. Van-Kieu Nguyen, Thuc Huy Duong, Tran Thanh Nha, Nguyen Ngoc Huyen Tran: data curation, visualization, investigation. Phan Nhat Minh, Nguyen

Tan Phat, Mai Thanh Chi, Dang Chi Hien: software, validation, supervision.

Conflicts of interest

The authors declare that they have no known competing financial interests or personal relationships that could have appeared to influence the work reported in this paper.

Acknowledgements

This work was supported by the Department of Science and Technology (DOST) of Dak Lak Province under grant number 369/HĐ-SKHCN. Research Lab for Drug Discovery and Development, University of Science, VNU-HCM, has supported the sample measurements.

References

1 A. Negi, M. Stephen, A. Vernon and D. M. Frcophth, *J. R. Soc. Med.*, 2003, **96**, DOI: 10.1258/Fjrsm.96.6.266.
2 M. Zhang, M. Chen, H. Q. Zhang, S. Sun, B. Xia and F. H. Wu, *Fitoterapia*, 2009, **80**, 475–477, DOI: 10.1016/j.fitote.2009.06.009.
3 T. Scully, *Nature*, 2012, **485**, S2–S3, DOI: 10.1038/485S2a.
4 P. S. N. Dong, H. V. T. Phan, J. Sichaem, H. V. N. Si, T. N. Tran, L. T. T. T. Hoang, T. M. S. Huynh, H. T. T. Le, D. T. Mai, T. L. Ngo, T. D. Le and V. K. Nguyen, *Nat. Prod. Res.*, 2024, **38**(16), 2869–2876, DOI: 10.1080/14786419.2023.2245958.
5 H. V. T. Phan, D. V. Nguyen, T. K. D. Le, T. A. M. Nguyen, P. S. N. Dong, T. N. Tran, N. V. T. Dao, H. C. Nguyen, H. T. Luu, W. Chavasiri, L. T. T. T. Hoang and V. K. Nguyen, *Nat. Prod. Res.*, 2024, 1–10, DOI: 10.1080/14786419.2024.2305659.
6 D. Kumar, V. Shah, R. Ghosh and B. C. Pal, *Nat. Prod. Res.*, 2013, **27**, 624–630, DOI: 10.1080/14786419.2012.686907.
7 M. H. Hoang, T. A. T. Nguyen, N. K. T. Pham, V. S. Dang and T. N. Vo, *Nat. Prod. Res.*, 2022, **36**, 5161–5167, DOI: 10.1080/14786419.2021.1921767.
8 L. F. Campuzano-Duque, J. C. Herrera, C. Ged and M. W. Blair, *Agronomy*, 2021, **11**, 1–13, DOI: 10.3390/agronomy11122550.
9 G. Oboh, O. M. Agunloye, S. A. Adefegha, A. J. Akinyemi and A. O. Ademiluyi, *J. Basic Clin. Physiol. Pharmacol.*, 2015, **26**, 165–170, DOI: 10.3390/agronomy11122550.
10 L. Castaldo, G. Graziani, A. Gaspari, L. Izzo, C. Luz, J. Mañes, M. Rubino, G. Meca and A. Ritieni, *J. Food Res.*, 2018, **7**, 43, DOI: 10.3390/Fmolecules25030631.
11 A. Heeger, A. K. Cagnazzo, E. Cantergiani and W. Andlauer, *Food Chem.*, 2017, **221**, 969–975, DOI: 10.1016/j.foodchem.2016.11.067.
12 S. Chase, N. Punbusayakul and M. F. Luang, *J. Process. Energy Agric.*, 2015, **19**, 224–227.
13 H. Mitiku, T. Y. Kim, H. Kang, E. Apostolidis, J. Y. Lee and Y. I. Kwon, *BMC Complementary Med. Ther.*, 2022, **22**, 249, DOI: 10.1186/s12906-022-03726-7.
14 V. Nguyen, E. G. Taine, D. Meng, T. Cui and W. Tan, *Nutrients*, 2024, **16**(7), 924, DOI: 10.3390/nu16070924.
15 A. Yosboonruang, A. Ontawong, J. Thapmamang and A. Duangjai, *J. Microbiol. Biotechnol.*, 2022, **32**, 1003–1010, DOI: 10.4014/jmb.2204.04003.
16 L. Wang, X. Pan, L. Jiang, Y. Chu, S. Gao, X. Jiang, Y. Zhang, Y. Chen, S. Luo and C. Peng, *Front. Nutr.*, 2022, **9**, DOI: 10.3389/fnut.2022.943911.
17 B. H. Li, X. F. Ma, X. D. Wu and W. X. Tian, *IUBMB Life*, 2006, **58**, 39–46, DOI: 10.1080/15216540500507408.
18 M. Miao and L. Xiang, *Advances in Pharmacology*, Academic Press Inc., 2020, vol. 87, pp. 71–88, DOI: 10.1016/bs.apha.2019.12.002.
19 R. Nowak, M. Drozd, E. Mendyk, M. Lemieszek, O. Krakowiak, W. Kisiel, W. Rzeski and K. Szewczyk, *Molecules*, 2016, **21**(7), 946, DOI: 10.3390/molecules21070946.
20 J. Zhao, Y. Mou, T. Shan, Y. Li, L. Zhou, M. Wang and J. Wang, *Molecules*, 2010, **15**, 7961–7970, DOI: 10.3390/molecules15117961.
21 P. Suttiarporn, W. Chumpolsri, S. Mahatheeranont, S. Luangkamin, S. Teepsawang and V. Leardkamolkarn, *Nutrients*, 2015, **7**, 1672–1687, DOI: 10.3390/nu7031672.
22 J. Sitkowski, L. Stefaniak, I. L. Nicol, M. L. Martin, G. J. Martin and G. A. Webb, *Spectrochim. Acta, Part A*, 1995, **51**(5), 839–841, DOI: 10.1016/0584-8539(94)00192-E.
23 M. J. Skowron, A. Z. Grześkowiak and T. Grześkowiak, *Eur. Food Res. Technol.*, 2015, **240**, 19–31, DOI: 10.1007/s00217-014-2356-z.
24 A. Farah, M. Monteiro, C. M. Donangelo and S. Lafay, *J. Nutr.*, 2008, **138**, 2309–2315, DOI: 10.3945/jn.108.095554.
25 N. E. Hachem, B. H. Kains, A. Khalil, F. H. Kobeissy and G. Nemer, *Methods in Molecular Biology*, Humana Press Inc., 2017, vol. 1598, pp. 391–403, DOI: 10.1007/978-1-4939-6952-4_20.
26 P. A. Ravindranath, S. Forli, D. S. Goodsell, A. J. Olson and M. F. Sanner, *PLoS Comput. Biol.*, 2015, **11**, 1–28, DOI: 10.1371/journal.pcbi.1004586.
27 E. W. Bell and Y. Zhang, *J. Cheminf.*, 2019, **11**(40), 1–9, DOI: 10.1186/s13321-019-0362-7.
28 K. Sargsyan, C. Grauffel and C. Lim, *J. Chem. Theory Comput.*, 2017, **13**, 1518–1524, DOI: 10.1021/acs.jctc.7b00028.
29 G. Giannini, W. Cabri, C. Fattorusso and M. Rodriquez, *Future Med. Chem.*, 2012, **4**, 1439–1460, DOI: 10.4155/fmc.12.80.
30 F. U. Eze, U. C. Okoro, D. I. Ugwu and S. N. Okafor, *Front. Chem.*, 2019, **7**, 1–12, DOI: 10.3389/fchem.2019.00634.
31 B. L. Staker, M. D. Feese, M. Cushman, Y. Pommier, D. Zembower, L. Stewart and A. B. Burgin, *J. Med. Chem.*, 2005, **48**, 2336–2345, DOI: 10.1021/jm049146p.
32 G. V. Vo, T. H. T. Nguyen, T. P. Nguyen, T. H. T. Do, N. M. A. Tran, H. T. Nguyen and T. T. Nguyen, *Saudi Pharmaceut. J.*, 2022, **30**, 1301–1314, DOI: 10.1016/j.jsps.2022.06.018.
33 H. T. Nguyen, T. T. Nguyen, T. H. Duong, N. M. A. Tran, C. H. Nguyen, T. H. A. Nguyen and J. Sichaem, *Molecules*, 2022, **27**(8), 2574, DOI: 10.3390/molecules27082574.

34 H. H. Nguyen, N. M. A. Tran, T. H. T. Nguyen, H. C. Vo, C. H. Nguyen, T. H. A. Nguyen, N. H. Nguyen and T. H. Duong, *J. Saudi Chem. Soc.*, 2022, **26**, 101489, DOI: **10.1016/j.jscs.2022.101489**.

35 N. K. T. Pham, N. M. A. Tran, H. T. Nguyen, D. D. Pham, T. Q. T. Nguyen, T. H. A. Nguyen, H. T. Nguyen, T. H. Do and N. H. Nguyen, *Arab. J. Chem.*, 2022, **15**, 103535, DOI: **10.1016/j.arabjc.2021.103535**.

36 S. H. Figueroa, A. R. Luévano, J. C. A. Pérez, A. G. Martínez, R. O. Andrade, I. L. Rivera and G. N. Vázquez, *Eur. J. Pharmacol.*, 2021, **15**, 174244, DOI: **10.1016/j.ejphar.2021.174244**.

37 E. S. Syamsul, S. Umar, F. S. Wahyuni, R. Martien and D. Hamidi, *Open Access Maced. J. Med. Sci.*, 2022, **10**, 1471–1477, DOI: **10.3889/oamjms.2022.10558**.

38 D. E. Shaw Research, *Desmond User's Guide Desmond Version 3.0/Document Version 0.5.3*, 2011.

39 X. Y. Meng, H. X. Zhang, M. Mezei and M. Cui, *Curr. Comput.-Aided Drug Des.*, 2011, **7**(2), 146–157, DOI: **10.2174/157340911795677602**.

40 J. Bhachoo and T. Beuming, *Methods Mol. Biol.*, 2017, 235–254, DOI: **10.1007/978-1-4939-6798-8_14**.

41 T. H. Duong, T. N. M. An, T. K. D. Le, T. M. D. Tran, H. T. Nguyen, T. H. A. Nguyen, N. H. Nguyen and J. Sichaem, *Nat. Prod. Res.*, 2024, **38**(15), 2603–2608, DOI: **10.1080/14786419.2023.2193746**.

42 N. H. Nguyen, Y. T. Vu, T. D. Nguyen, T. T. Cao, H. T. Nguyen, T. K. D. Le, J. Sichaem, D. T. Mai, T. N. M. An and T. H. Duong, *RSC Adv.*, 2023, **13**, 35408–35421, DOI: **10.1039/D3RA06760B**.

43 G. Xiong, Z. Wu, J. Yi, L. Fu, Z. Yang, C. Hsieh, M. Yin, X. Zeng, C. Wu, A. Lu, X. Chen, T. Hou and D. Cao, *Nucleic Acids Res.*, 2021, **49**, W5–W14, DOI: **10.1093/nar/gkab255**.

44 M. Bitew, T. B. Tegene Demissie, A. Belayneh, M. Endale and R. Eswaramoorthy, *PLoS One*, 2021, **16**(12), e0260853, DOI: **10.1371/journal.pone.0260853**.

45 Y. Wang, J. Xing, Y. Xu, N. Zhou, J. Peng, Z. Xiong, X. Liu, X. Luo, C. Luo, K. Chen, M. Zheng and H. Jiang, *Q. Rev. Biophys.*, 2015, **48**, 488–515, DOI: **10.1017/s0033583515000190**.

46 L. J. Shai, S. R. Magano, L. S. Lebelo and M. A. Mogale, *J. Med. Plants Res.*, 2011, **5**, 2863–2867.

47 N. Duy, T. Ha, T. Phuong, N. Van Cuong and T. N. M. An, *ChemistrySelect*, 2023, **8**, e202300246, DOI: **10.1002/slct.202300246**.

48 T. C. Mai, N. T. Tran, D. T. Mai, T. T. N. Mai, N. H. T. Duyen, T. N. M. An, M. Alam, C. H. Dang and T. D. Nguyen, *RSC Adv.*, 2022, **12**, 25962–25976, DOI: **10.1039/D2RA04068A**.

49 S. U. Khan, N. Ahemad, L. H. Chuah, R. Naidu and T. T. Htar, *Progress in Drug Discovery & Biomedical Science*, 2020, **3**(1), 1–21, DOI: **10.36877/pddbs.a0000054**.

50 M. Y. Putra, G. Bavestrello, C. Cerrano, B. Renga, C. D'Amore, S. Fiorucci, E. Fattorusso and O. Taglialatela-Scafati, *Steroids*, 2012, **77**, 433–440, DOI: **10.1016/j.steroids.2011.12.026**.

51 T. Orita, S. Chogahara, M. Okuda, K. Sakao, T. Miyata and D. X. Hou, *Foods*, 2023, **12**(13), 2611, DOI: **10.3390/foods12132611**.

52 K. Eawsakul, P. Panichayupakaranant, T. Ongtanasup, S. Warinhomhoun, K. Noonong and K. Bunluepuech, *Heliyon*, 2021, **7**(9), e08078, DOI: **10.1016/j.heliyon.2021.e08078**.

53 G. Oboh, O. M. Agunloye, S. A. Adefegha, A. J. Akinyemi and A. O. Ademiluyi, *J. Basic Clin. Physiol. Pharmacol.*, 2015, **26**, 165–170, DOI: **10.1515/jbcpp-2013-0141**.

54 K. Chen, C. Peng, F. Chi, C. Yu, Q. Yang and Z. Li, *Front. Microbiol.*, 2022, **13**, DOI: **10.3389/fmicb.2022.885092**.

55 F. Kabir, S. Katayama, N. Tanji and S. Nakamura, *J. Korean Soc. Appl. Biol. Chem.*, 2014, **57**, 359–365, DOI: **10.1007/s13765-014-4056-6**.